Chemical Science

ROYAL SOCIETY OF CHEMISTRY

EDGE ARTICLE

View Article Online
View Journal | View Issue

Cite this: *Chem. Sci.*, 2024, **15**, 3571

All publication charges for this article have been paid for by the Royal Society of Chemistry

Received 8th November 2023
Accepted 16th January 2024

DOI: 10.1039/d3sc06004g

rsc.li/chemical-science

Rapid, high-capacity adsorption of iodine from aqueous environments with amide functionalized covalent organic frameworks†

Niyati Arora,[a] Tanay Debnath,[b] Milinda C. Senarathna,[a] Rebecca M. Johnson,[a] Isabella G. Roske,[a] G. Andrés Cisneros *[ab] and Ronald A. Smaldone *[a]

The uses and production of radionuclides in nuclear energy production and medical therapy are becoming more significant in today's world. While these applications have many benefits, they can produce harmful pollutants, such as radioactive iodine, that need to be sequestered. Effective capture and storage of radioactive iodine waste remains a major challenge for nuclear energy generation and nuclear medicine. Here we report the highly efficient capture of iodine in a series of mesoporous, two-dimensional (2D) covalent organic frameworks, called COFamides, which contain amide sidechains in their pores. COFamides are capable of rapidly removing iodine from aqueous solution at concentrations as low as 50 ppm, with total capacities greater than 650 wt%. In order to explain the high affinity of the COFamide series for iodine and iodide species in water, we performed a computational analysis of the interactions between the COFamide framework and iodine guests. These studies suggest that the origin of the large iodine capacity in these materials can be explained by the presence of multiple, cooperative, non-covalent interactions between the framework and both iodine, and iodide species.

Introduction

Iodine pollution from nuclear and medical waste (^{129}I and ^{131}I) is a problem for both humans and the environment due to its ability to accumulate in waterways, soil or in certain tissues, especially in the thyroid gland. Radioactive iodine is a major pollutant in nuclear accidents such as the Fukushima,[1] and Chernobyl nuclear power plant disasters as well as regular nuclear waste disposal from power generation facilities.[2–4] In fact, after 1986, thyroid cancer cases spiked tremendously among the people living in vicinity of the Chernobyl power plant.[5] The biomagnification of radioactive iodine species among the local population, particularly children,[1] was determined to be the cause of disease proliferation. Additionally, excessive iodine consumption (1.1 mg per day) on a regular basis can potentially cause thyroid problems, including cancer.[6] In addition to its ability to affect human health, ^{129}I has a very long half-life of ~10 million years.[7,8] Therefore, it is vital and necessary to develop new materials for iodine capture given the detrimental impacts. Current methods for removing radioactive iodine from different industrial waste streams include wet scrubbing (using alkaline solutions like NaOH or $Hg(NO_3)_2$) as well as solid phase adsorption (using silver salts, zeolites, minerals containing bismuth oxyiodide, activated carbon and others).[9,10] However, these methods have drawbacks such as the need for complex equipment, hazardous by product generation, poor absorption capacities, and high cost because of the need for expensive sorbents.[7,11–13] For these reasons, the development of alternative, chemically stable materials that can collect iodine at low concentrations in aqueous environments, remains a key challenge.

To address this problem, researchers have begun to explore the vast library of porous organic materials as high-performance adsorbents for iodine pollution. Covalently linked networks such as porous organic polymers (POPs), covalent organic frameworks (COFs) and others have demonstrated excellent uptake of iodide, triiodide and iodine species.[11,14–16] COFs are a class of polymers, that have exceptional crystallinity, and high surface areas that can be designed with pore apertures ranging from 1–10 nm.[17–23] These characteristics have excellent prospective applications in the fields of energy, catalysis,[24,25] gas storage,[26,27] and separation.[28,29] COFs have received a lot of attention recently in the field of iodine vapor adsorption because of their porous structures, uniform channels, high accessible surface area, and highly conjugated structures.[20–23] Although some progress has been made in capturing the radioactive iodine from water, currently, it is

[a]*Department of Chemistry and Biochemistry, University of Texas, Dallas, 800 W. Campbell Rd, Richardson, Texas 75080, USA. E-mail: ronald.smaldone@utdallas.edu; andres@utdallas.edu*

[b]*Department of Physics, University of Texas, Dallas, 800 W. Campbell Rd, Richardson, Texas 75080, USA*

† Electronic supplementary information (ESI) available. See DOI: https://doi.org/10.1039/d3sc06004g

challenging to remove the low concentration of iodide and triiodide ions from water (~10 ppm).[30,31]

The porous adsorbent must have high affinities for both iodine and iodide species and wide voids for high capacitive adsorption in order to quickly remove these pollutants from water where they are often found in low concentrations. For the removal of iodine, a number of porous materials, including metal–organic frameworks (MOFs),[11,32,33] organic polymers,[4,33–35] and hydrogen-bonded organic frameworks (HOFs),[31,36,37] have recently been reported. However, one major challenge that remains in this area involves the removal of I^- and I_3^- at low concentrations in aqueous environments.[30] Previously reported efforts employing hydrogen-bonded crosslinked organic frameworks HcOFs, MOFs, COFs, and POPs can remove large amounts of iodine from aqueous environments.[7,30,31,38] In these studies, iodide (I^-) is added to water to stabilize iodine (I_2) *via* $I_2 + I^- \rightleftharpoons I_3^-$ equilibrium.[30,31] However, many of these systems work best at removing molecular iodine (I_2) at higher concentrations (>100 ppm) in water. In practice, the residual iodine levels (5–16 ppm) in treated water are substantially lower than these concentrations. Examples of porous framework materials that can simultaneously remove both iodine and iodide at low concentrations remain rare. In this report, we carried out experiments which demonstrate the ability of amide functionalized COFs to absorb iodine as well as iodide species and sequester them with high capacities, and computational simulations to investigate the atomic and electronic factors underpinning the interactions between different iodide species and the COFs.

Results and discussion

We have used two imine-linked COFs[17,39] (COFamide-2 and PyCOFamide) and one azine-linked COF (COFamide-1)[39] shown in Fig. 1(A) for the removal of iodine from aqueous solutions. These COFs were synthesized according to previously reported literature.[17,39] COFamides have amide sidechains that are capable of acting as hydrogen-bonding donors and acceptors which stabilize their large porous structures. COFamide-1, COFamide-2, and PyCOFamide have high Brunauer, Emmett and Teller (BET) surface areas of (1202, 1390 and 1909) $m^2\ g^{-1}$ respectively, and pore sizes of 23 Å, 33 Å, and 65 Å respectively as measured in our previous reports.[17,39] While many porous organic materials are constructed largely from rigid, aromatic components, COFamides also contain secondary hexylamide groups which can donate or accept hydrogen bonds and provide hydrophobic interactions through their *n*-hexyl chains.[17] This molecular construction allows them to potentially interact with neutral iodine or iodide species (Fig. 1(B)).

The iodine absorption ability of all three COFamides was determined using time-dependent UV/vis measurements. Each COFamide (3.0 mg) was added to a saturated aqueous iodine solution (*ca.* 1.2 mM) shown in Fig. 2(A)–(C). The inset image in Fig. 2 shows that the color of the COFamide powders changed from yellow to brown upon addition to the iodine water for 24 h, indicating that iodine was absorbed. The time dependent UV/vis measurements for all the three COFs showed a decrease in the absorbance peaks of iodide (290 nm) and triiodide anions (355 nm) within 30 min (Fig. 2(A)–(C)). These experiments showed a decrease in iodine concentration from 40 ppm to less than 20 ppm within 30 min and below 1, 5.95 and 8.89 ppm after 24 h, for COFamide-1, COFamide-2, and PyCOFamide respectively (Fig. 2(D)). This indicates that these three COFs were able to decrease the iodine concentration to less than 10 ppm within 24 h.[30] COFamide-1, which has the smallest pores amongst the three, absorbs iodine at faster initial rate than the other two COFamides. We hypothesize that this can be explained by its higher concentration of functional groups in the pores due to its smaller pore diameter compared to the other COFamides.

Since several of the functional groups in the COFamides can form non-covalent interactions with anionic iodine species, we hypothesized that the exceptional adsorption properties of the COFamides could be related to their ability to bind to iodide and triiodide and drive the equilibrium towards I_2 within the pores of the COFs. In fact, aqueous anion recognition in porous polymers has been observed previously where amides, or other designed supramolecular receptors, are incorporated into the porous structure.[40–44] To demonstrate the potential for iodide binding in the mechanism of iodine adsorption in COFamides, we dissolved potassium iodide in water and the time dependent UV/vis measurements were done at the interval of 5 min up-to 15 min and then up to 30 min, and the decrease in the peak at 230 nm was observed. The reduction of this peak shows that COFamides are capable of absorbing iodide (I^-) by either binding to the amide groups or through anion–π interactions with the linkers on the pore walls, or at defect sites (Fig. 3(A)). The maximum iodine absorption capacity of COFamides in an aqueous solution was measured to be 6.53 ± 0.2 g, 5.91 ± 0.2 g, 4.62 ± 0.2 g of iodine per 1 g of PyCOFamide, COFamide-2, COFamide-1 respectively (Fig. 2(E) and S5(a)–(c)†). These values were measured by immersing the COF powders in a concentrated aqueous solution of KI_3 for five days as shown in Fig. S3,† where I_2 is generated *in situ* through the following reaction: $I_3^- \leftrightarrows I_2 + I^-$ which occurs under equilibrium. The presence of iodine was detected in solid samples collected after the adsorption experiment by energy dispersive spectroscopy (EDS, Fig. S11†). The presence of iodine was detected in solid samples collected after the adsorption experiment by energy dispersive spectroscopy (EDS, Fig. S11†). Thermogravimetric analysis was performed (Fig. S12†) to observe the strength of guest–framework interactions as well as the thermal framework stability.

While the initial kinetics of the adsorption are faster for the smaller pore COF, PyCOFamide, with the biggest pore size amongst the three COFamides, exhibits the largest maximum capacity for iodine. The larger pore volume is likely a major contributor to this observation, however PyCOFamide is different from the other materials studied here in that its linker is based on a larger aromatic linker (pyrene). Previous studies of other porous polymers that have excellent affinities for iodine have shown that larger aromatic components can participate in the iodine absorption *via* charge-transfer complexes formed with the p-orbitals of iodine or iodidies.[5]

Additionally, to directly observe the interactions between the framework and the iodine, we used Fourier transform infrared spectroscopy (FT-IR). When the FT-IR spectra of the iodine

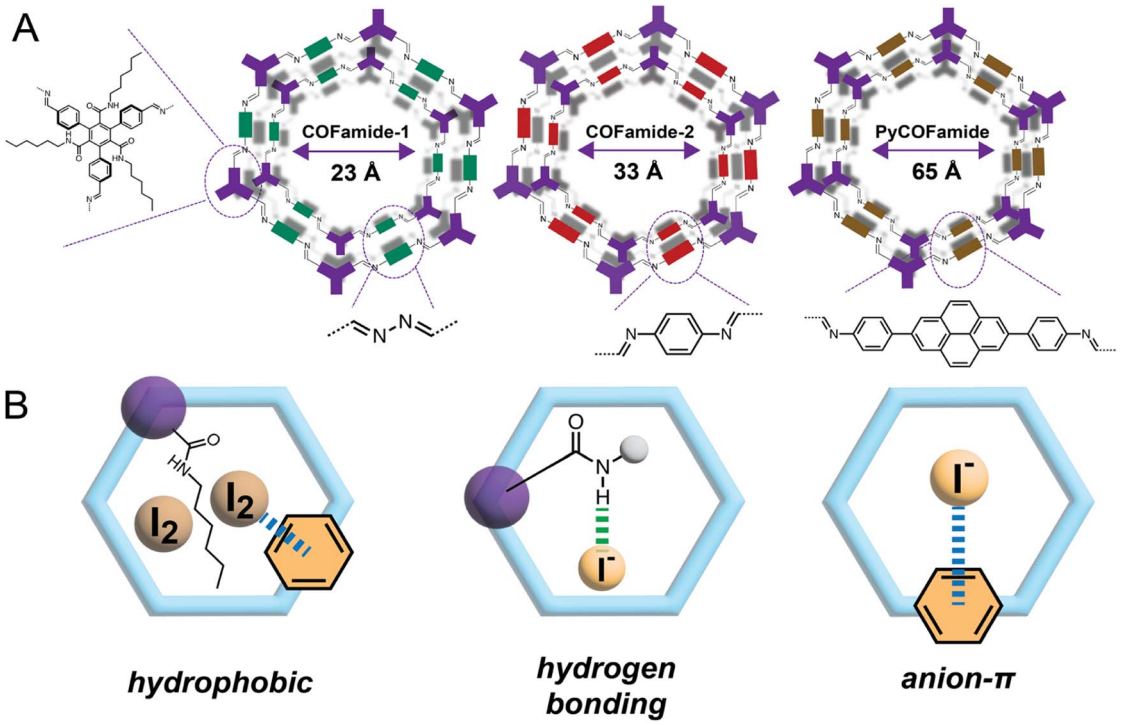

Fig. 1 (A) Structures and pore sizes of the COFamides used in this study. (B) Illustrations of the types of non-covalent interactions between the framework and iodine guests that are possible within the COFamide pores.

loaded COFamide was compared to the COFamide before adsorption, it was found that the one with iodine loading exhibits enhanced N–H stretching vibrations, as shown in Fig. 3(B), the centre of the peak shifted from 3305 to 3292 cm^{-1}, with increasing uptake of iodine. This is indicative of non-covalent interactions between the free amide groups in the COF

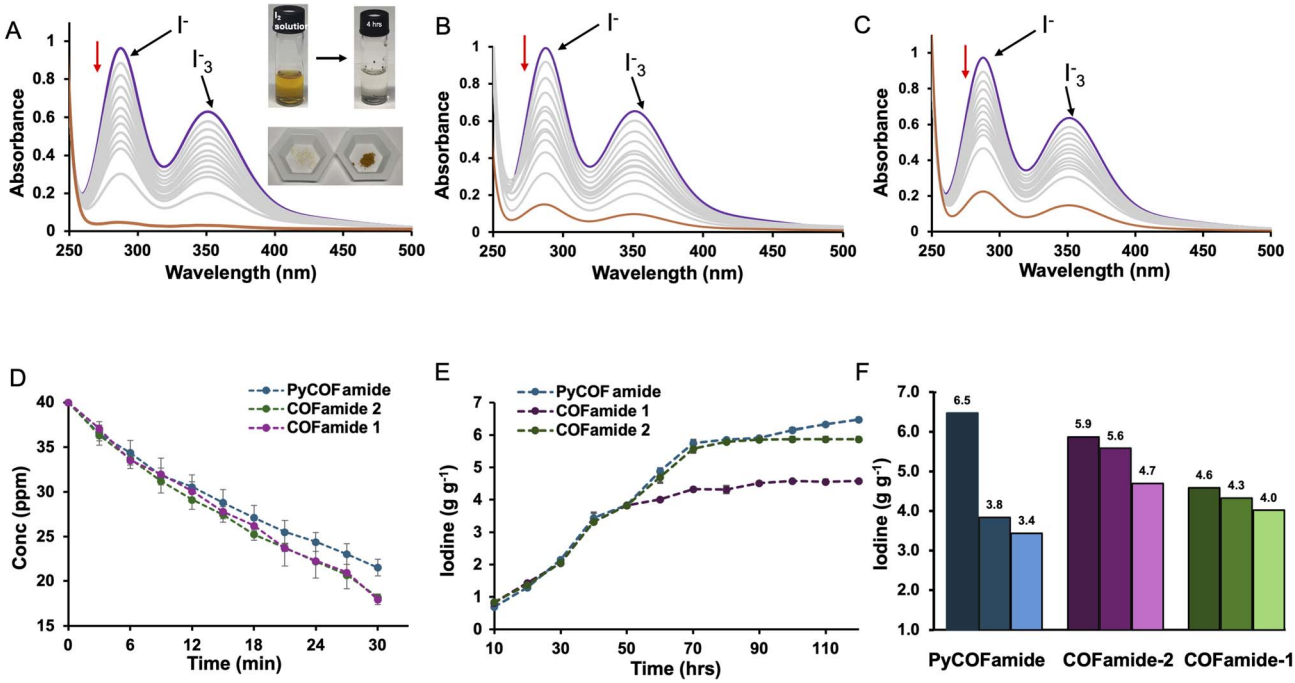

Fig. 2 Time dependent UV-vis absorption spectra of an aqueous solution of (1.2 mM) upon addition of (A) COFamide-1 (3.0 mg) (B) COFamide-2 (3.0 mg) and (C) PyCOFamide (3.0 mg). Purple: I_2 saturated aqueous solution, $t = 0$ min, grey: $t =$ every 3 min, brown: $t = 4$ h (D) I_2 concentration decrease after 30 min of adding COFamide (E) maximum iodine capacity measurements for all three COFamides (F) iodine uptake capacity of COFamides for up to three cycles.

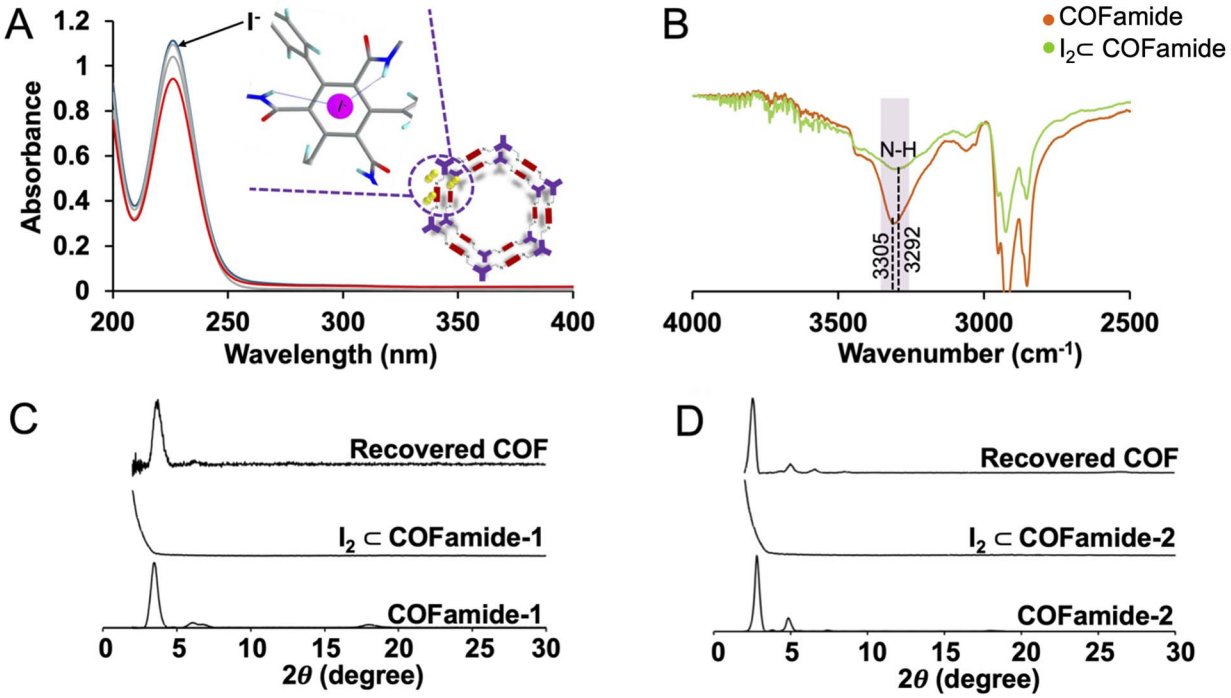

Fig. 3 (A) Adsorption of iodide in COFamide upon addition of KI_3 in water. Blue: I_2 saturated aqueous solution, $t = 0$ min, grey: $t =$ every 5 min, red: $t = 30$ min (B) FT-IR of COFamide-2 (C) PXRD of COFamide-1 and (D) COFamide-2 before and after the iodine uptake.

structure with iodine. Furthermore, to ratify the role of amide bonds in the iodine absorption of COFamides we did a control experiment using Me-COFs which is symmetrically similar to COFamides, but instead of amide groups, there are now methyl groups attached, was detected under the same conditions. The results disclosed that, despite the fact that the control itself possesses similar pore size, it displays a low iodine adsorption capacity as compared to COFamides as shown in Fig. S6,† which could be attributed to the absence of effective interaction between free amide rich sites and iodine species. Regardless of the fact that these control COFs are not particularly superlative in terms of iodine adsorption capacity collateral with the COFamides, more than 45% capacity enhancement in iodine uptake capacity over the control COFs should appear by introducing nitrogen-rich amide sites into the frameworks. Furthermore, we compared the maximum iodine absorption of COFamides to some polymers already present in literature and found that these COFamides are contesting with the maximum absorption of some polymers that absorb iodine in gas phase while COFamides compete with them in liquid phase. The comparison table of the same is shown in Table S1.†

To determine the reusability of these COFamides for repeated iodine absorption, we immersed the loaded COFamides in ethanol and dimethyl sulfoxide (DMSO), and monitored the release of iodine by UV/vis. More than 95% of the encapsulated iodine was released within 30 min demonstrating the reversible interactions between the absorbed iodine and the COFamide structure. Release data of COFamides in ethanol and DMSO is shown in Fig. S7(A) and (B).† The speed of release is slower in DMSO than the ethanol because of difference of solubility of iodine in these two solvents. The recovered COF was reactivated using supercritical carbon dioxide ($scCO_2$) to remove the residual ethanol or DMSO and the PXRD patterns of the recovered COF powders were compared to the materials before iodine adsorption. The original crystalline structures were preserved, for COFamides1–2, Fig. 3(C) and (D), but PyCOFamide was found to be amorphous after the first regeneration cycle shown in Fig. S10(C).† A previous example where reversible crystallinity in iodine adsorption was observed attributed this phenomenon to structural flexibility, where the adsorbent can reorganize back to the original structure after the iodine is removed.[31] We hypothesize a similar situation where the order of the structure can be disrupted by competition with iodine molecules or iodide anions for the interlayer amide hydrogen bonding interactions. Disruption of these hydrogen bonds could lead to a less crystalline COF structure, which can be regenerated after the iodine is removed. All three COFamides were tested in three absorption and desorption cycles. COFamide 1 and 2 retain most of their adsorption capability after three cycles, however PyCOFamide was considerably decreased, though it still could remove a significant amount of iodine (>3 g g^{-1}). COFamides1–2 are known to be resistant to pore collapse, whereas PyCOFamide must be activated with $scCO_2$.[17] While we suspect that the reduction in iodine adsorption capability in PyCOFamide is due to delamination or pore collapse during the reactivation process, it is interesting to note that the intact pore structure appears to play a large role in the adsorption behaviour, rather than just the overall density of the functional groups capable of forming non-covalent interactions with iodine guests.

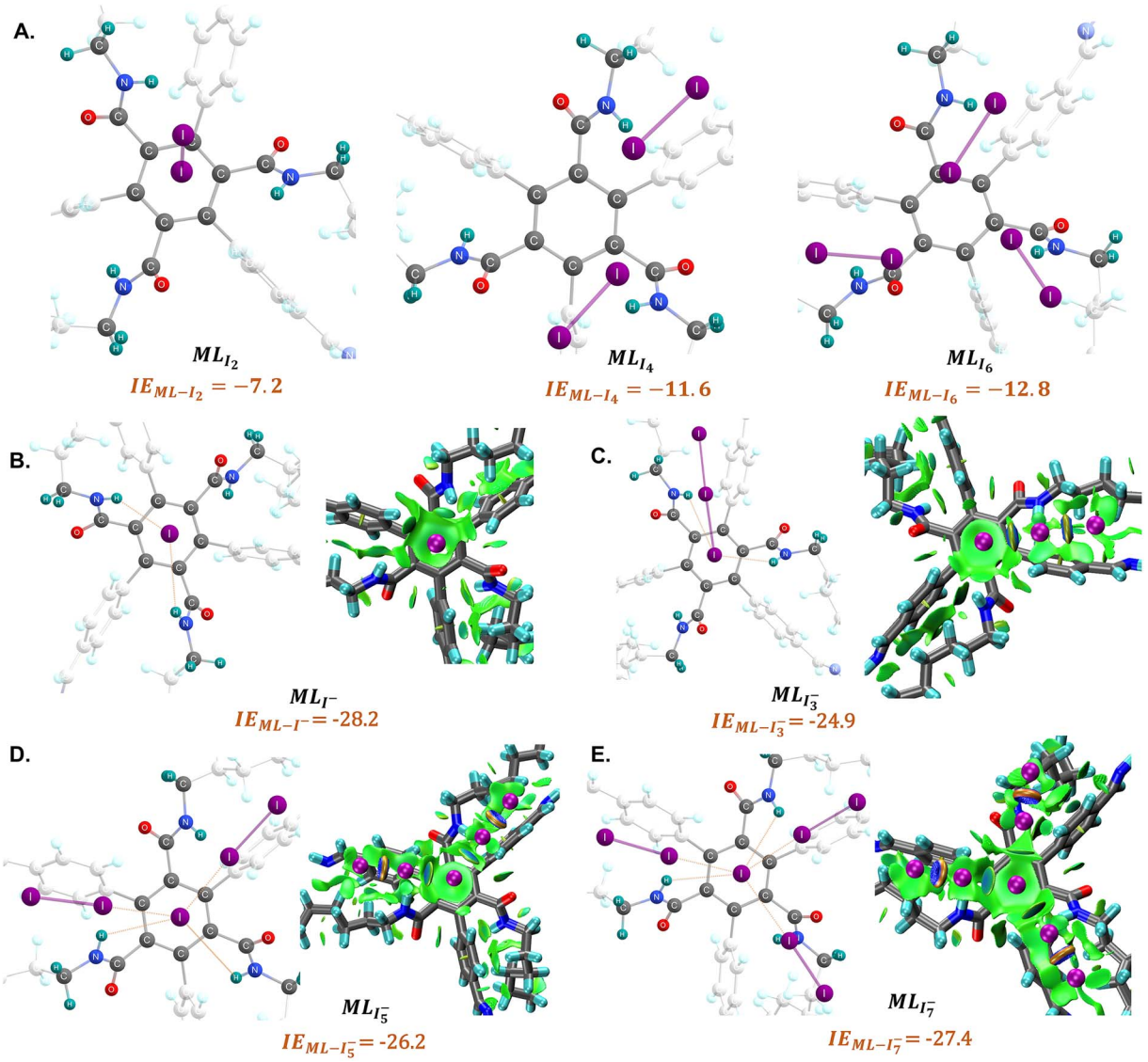

Fig. 4 Constrained optimized geometries of (A) I_2 ($\mathbf{ML_{I_2}}$) (left), I_4 ($\mathbf{ML_{I_4}}$) (middle), I_6 ($\mathbf{ML_{I_6}}$) (right). (B) I^- ($\mathbf{ML_{I^-}}$), (C) I_3^- ($\mathbf{ML_{I_3^-}}$), (D) I_5^- ($\mathbf{ML_{I_5^-}}$), (E) I_7^- ($\mathbf{ML_{I_7^-}}$) and their topological diagram of non-covalent interaction plot on monomeric unit of COF at WB97XD/6-31+G(D) (C,H,N,O)/DEF2SVP(I). Interaction energies are in kcal mol^{-1} (green surfaces represent the attractive non-covalent interactions).

We have further investigated iodine–COF interactions by considering monolayer and bilayer models of the COF unit *via* DFT simulations and COF models with and without amide bonds (Computational methodology in ESI†). Two major outcomes from experiments have been further supported by the computations: (1) linker size *vs.* iodine uptake capacity, (2) significance of amide bonds on iodine capture. As depicted in Fig. S13,† the interaction energy (IE) of I_2 in different binding modes associated with the different linkers are observed to be larger for pyrene likely due to its larger size and extended aromaticity (IE link-I_2 −6.1 kcal mol^{-1} and −5.5 kcal mol^{-1} for PYR1 and PYR2 respectively) as compared to benzene (IE link-I_2 −4.5 kcal mol^{-1} for BENZ1). Thus, our computational results support the hypothesis of a proportional relationship between pore size and I_2 uptake capacity. Molecular level inspection of the influence of amide bonds on iodine capture has been studied computationally by considering the interaction between different iodine nuclear complexes (I^-, I_2, I_3^- ESI† and Fig. 4). Several different binding modes of the different iodine molecules in the COF were investigated. As shown in (Fig. 4), the amide bond-containing monolayer COF model shows larger interaction energies, $IE_{COF-I^-} = -28.2$ kcal mol^{-1} and $IE_{COF-I_3^-} = -24.9$ kcal mol^{-1} for anionic iodine molecules. Conversely, the COF monolayer model without amide bonds (Fig. S14†) shows reduced interaction energies of $IE_{COF-I^-} = -14.9$ kcal mol^{-1} and $IE_{COF-I_3^-} = -16.4$ kcal mol^{-1}. We have also considered a bilayer COF model to investigate the iodine uptake process which also shows analogous results as those observed for the monolayer, further supporting the uptake of anionic iodine molecular forms as shown in Fig. S15.† Structural analysis indicates that iodine can orient in proximity to the exposed NH groups so that it can form N–H–I interactions. The existence of this N–H–I interaction is further supported by symmetry adapted perturbation theory.

Our SAPT(DFT) analysis indicates that the electrostatic (-24.9 kcal mol^{-1}) and induction energy (-15.4 kcal mol^{-1}) components are the major contributing terms for the total interaction energy Table S2.† Non-covalent index (NCI) analysis further supports the observed interaction between NH and iodine as visualized prominently for I^- and I_3^- (Fig. 4). It should be mentioned that NCI also portrays the non-covalent interactions between other parts of the COF and iodine mostly concentrated on the core benzene, indicating many-body effects play an important role in the interaction between the guest and the host.

Interestingly, for neutral I_2, both COFs with and without amide-bonds, show IEs that are up to three times lower in magnitude. For I_2, SAPT shows dispersion (-7.4 kcal mol^{-1}) is the major contributing term despite the presence of polar amides bonds. Low IE with insignificant contribution of electrostatic and induction energy as shown in Table S2† suggests that iodine as neutral form shows low uptake capacity regardless of the presence of the amide bond.

Taken together, these results suggest that anionic iodine moieties facilitate the uptake of iodine by the COF through NH–I interactions. This was further confirmed by modeling multiple I_2 capture with and without an anionic iodine counterpart. These structures have been previously reported as possible binding modes based on Raman spectroscopy.[2,5,33] The tested models show that the presence of a single I^- promotes strong interaction energies of multiple iodine molecules ($2I_2$ and $3I_2$) with the amide bond-containing COF, whereas the absence of the anionic iodine shows significantly smaller interaction energies (Fig. 4). The optimized structures suggest that I_2 molecules are oriented in the proximity of I^- so that they can form a I^-–xI_2 ($x = 2$, 3) network. NCI plot analysis suggests significant non-covalent interactions between I^- and the I_2 molecules. SAPT(DFT) analysis (Table S2†) suggests that electrostatic (-54.2 kcal mol^{-1}) and induction energies (-50.4 kcal mol^{-1}) are the major contributing terms in total interaction energy between COF–I^- and $2I_2$. This suggests the possible capture of multiple iodine molecules inside the COF *via* NH–I^-–I_2 interactions; the importance of many-body effects between host and guest.

Conclusion

In summary, we have carried out an in-depth study of iodine adsorption in amide functionalized 2D-COFs. Iodine can be rapidly removed from aqueous solutions at both high, and low concentrations using all three COFamides. We demonstrated that the pore size can contribute to the overall adsorption capacity, and that loss of the crystalline structure of the COF can significantly reduce its adsorption capability. Computational studies suggest possible binding sites of different iodine species (both I_2 and iodide) inside the COF with the prediction of active participation of the linker groups (–NH and aromatic moieties). These studies also infer the facilitation of iodine capture is driven though generation of NH–I^- interactions with the amide sidechains. Overall, this work shows that in order to design a porous material capable of high-performance adsorption of iodine species from aqueous environments, it is necessary to take a multivariate approach that includes designed supramolecular interactions, and considers all possible forms of iodine, both ionic and molecular.

Data availability

XYZ files of the geometries are provided as ESI.†

Author contributions

The manuscript was written through contributions of all authors. All authors have given approval to the final version of the manuscript.

Conflicts of interest

There are no conflicts to declare.

Acknowledgements

This work was funded by the American Chemical Society Petroleum Research Fund (PRF#61360-ND10) to RAS, the National Institutes of Health through R01GM108583 to GAC, and Fulbright-Nehru Postdoctoral Fellowship to TD. Computing time from XSEDE through allocation TG-CHE160044 and UNT CASCaM (partially funded by NSF Grant No. CHE1531468 and OAC-2117247) is gratefully acknowledged.

Notes and references

1 M. H. Nadesan, *Fukushima and the Privatization of Risk*, Palgrave Macmillan, 2013.
2 Z. Wang and Y. Huang, *Nouv. J. Chim.*, 2023, **47**, 3668–3671.
3 S. Ruidas, A. Chowdhury, A. Ghosh, A. Ghosh, S. Mondal, A. D. D. Wonanke, M. Addicoat, A. K. Das, A. Modak and A. Bhaumik, *Langmuir*, 2023, **39**, 4071–4081.
4 Y. Liao, J. Weber, B. M. Mills, Z. Ren and C. F. J. Faul, *Macromolecules*, 2016, **49**, 6322–6333.
5 A. Hassan and N. Das, *ACS Appl. Polym. Mater.*, 2023, **5**, 5349–5359.
6 M. A. Greer, G. Goodman, R. C. Pleus and S. E. Greer, *Environ. Health Perspect.*, 2002, **110**, 927–937.
7 W. Xie, D. Cui, S. R. Zhang, Y. H. Xu and D. L. Jiang, *Mater. Horiz.*, 2019, **6**, 1571–1595.
8 Q. Wang, H. Yu, X. Chen and Y. He, *Adv. Funct. Mater.*, 2023, **33**, 2300487.
9 B. J. Riley, J. D. Vienna, D. M. Strachan, J. S. McCloy and J. L. Jerden, *J. Nucl. Mater.*, 2016, **470**, 307–326.
10 T. S. Chee, Z. Tian, X. Zhang, L. Lei and C. Xiao, *J. Nucl. Mater.*, 2020, **542**, 152526.
11 X. Zhang, J. Maddock, T. M. Nenoff, M. A. Denecke, S. Yang and M. Schröder, *Chem. Soc. Rev.*, 2022, **51**, 3243–3262.
12 L. Wang, Z. Li, Q. Wu, Z. Huang, L. Yuan, Z. Chai and W. Shi, *Environ. Sci.: Nano*, 2020, **7**, 724–752.
13 T. Pan, K. Yang, X. Dong and Y. Han, *J. Mater. Chem.*, 2023, **11**, 5460–5475.

14 Q. Sun, B. Aguila and S. Ma, *Trends Chem.*, 2019, **1**, 292–303.
15 G. Das, T. Skorjanc, S. K. Sharma, F. Gándara, M. Lusi, D. S. Shankar Rao, S. Vimala, S. Krishna Prasad, J. Raya, D. S. Han, R. Jagannathan, J. C. Olsen and A. Trabolsi, *J. Am. Chem. Soc.*, 2017, **139**, 9558–9565.
16 H. Zuo, W. Lyu, W. Zhang, Y. Li and Y. Liao, *Macromol. Rapid Commun.*, 2020, **41**, e2000489.
17 S. D. Diwakara, W. S. Y. Ong, Y. H. Wijesundara, R. L. Gearhart, F. C. Herbert, S. G. Fisher, G. T. McCandless, S. B. Alahakoon, J. J. Gassensmith, S. C. Dodani and R. A. Smaldone, *J. Am. Chem. Soc.*, 2022, **144**, 2468–2473.
18 P. W. Anderson, W. F. Brinkman and D. A. Huse, *Science*, 2005, **310**, 1164–1166.
19 H. R. Abuzeid, A. F. M. EL-Mahdy and S. W. Kuo, *Giant*, 2021, **6**, 100054.
20 Y. Zhai, G. Liu, F. Jin, Y. Zhang, X. Gong, Z. Miao, J. Li, M. Zhang, Y. Cui, L. Zhang, Y. Liu, H. Zhang, Y. Zhao and Y. Zeng, *Angew. Chem., Int. Ed.*, 2019, **131**, 17843–17847.
21 Z. Wang, S. Zhang, Y. Chen, Z. Zhang and S. Ma, *Chem. Soc. Rev.*, 2020, **49**, 708–735.
22 Y. Li, W. Chen, G. Xing, D. Jiang and L. Chen, *Chem. Soc. Rev.*, 2020, **49**, 2852–2868.
23 P. J. Waller, F. Gándara and O. M. Yaghi, *Acc. Chem. Res.*, 2015, **48**, 3053–3063.
24 H. Xu, X. Chen, J. Gao, J. Lin, M. Addicoat, S. Irle and D. Jiang, *Chem. Commun.*, 2014, **50**, 1292–1294.
25 S. Lin, C. S. Diercks, Y. B. Zhang, N. Kornienko, E. M. Nichols, Y. Zhao, A. R. Paris, D. Kim, P. Yang, O. M. Yaghi and C. J. Chang, *Science*, 2015, **349**, 1208–1213.
26 H. Furukawa and O. M. Yaghi, *J. Am. Chem. Soc.*, 2009, **131**, 8875–8883.
27 H. Ma, H. Ren, S. Meng, Z. Yan, H. Zhao, F. Sun and G. A. Zhu, *Chem. Commun.*, 2013, **49**, 9773–9775.
28 M. S. Lohse, T. Stassin, G. Naudin, S. Wuttke, R. Ameloot, D. De Vos, D. D. Medina and T. Bein, *Chem. Mater.*, 2016, **28**, 626–631.
29 S. Kandambeth, B. P. Biswal, H. D. Chaudhari, K. C. Rout, H. S. Kunjattu, S. Mitra, S. Karak, A. Das, R. Mukherjee, U. K. Kharul and R. Banerjee, *Adv. Mater.*, 2017, **29**, 1603945.
30 M. Zhang, J. Samanta, B. A. Atterberry, R. Staples, A. J. Rossini and C. Ke, *Angew. Chem., Int. Ed.*, 2022, **61**, e202214189.
31 Y. Lin, X. Jiang, S. T. Kim, S. B. Alahakoon, X. Hou, Z. Zhang, C. M. Thompson, R. A. Smaldone and C. Ke, *J. Am. Chem. Soc.*, 2017, **139**, 7172–7175.
32 D. F. Sava, M. A. Rodriguez, K. W. Chapman, P. J. Chupas, J. A. Greathouse, P. S. Crozier and T. M. Nenoff, *J. Am. Chem. Soc.*, 2011, **133**, 12398–12401.
33 Z. Yin, Q. X. Wang and M. H. Zeng, *J. Am. Chem. Soc.*, 2012, **134**, 4857–4863.
34 K. Su, W. Wang, B. Li and D. Yuan, *ACS Sustain. Chem. Eng.*, 2018, **6**, 17402–17409.
35 S. Huang, J. Y. Choi, Q. Xu, Y. Jin, J. Park and W. Zhang, *Angew. Chem., Int. Ed.*, 2023, **62**, e202303538.
36 X. Song, Y. Wang, C. Wang, D. Wang, G. Zhuang, K. O. Kirlikovali, P. Li and O. K. Farha, *J. Am. Chem. Soc.*, 2022, **24**, 10663–10687.
37 I. Hisaki, N. Ikenaka, E. Gomez, B. Cohen, N. Tohnai and A. Douhal, *Chem.–Eur. J.*, 2017, **23**, 11611–11619.
38 K. Cheng, H. Li, Z. Li, P. Z. Li and Y. Zhao, *ACS Mater. Lett.*, 2023, **5**, 1546–1555.
39 S. B. Alahakoon, K. Tan, H. Pandey, S. D. Diwakara, G. T. McCandless, D. I. Grinffiel, A. Durand-Silva, T. Thonhauser and R. A. Smaldone, *J. Am. Chem. Soc.*, 2020, **142**, 12987–12994.
40 W. S. Y. Ong, R. A. Smaldone and S. C. Dodani, *Chem. Sci.*, 2020, **11**, 7716.
41 A. Jrad, M. A. Olson and A. Trabolsi, *Chem*, 2023, 1413–1451.
42 H. Wang, L. O. Jones, I. Hwang, M. J. Allen, D. Tao, V. M. Lynch, B. D. Freeman, N. M. Khashab, G. C. Schatz, Z. A. Page and J. L. Sessler, *J. Am. Chem. Soc.*, 2021, **143**, 20403–20410.
43 W. Lin, G. Zhang, X. Zhu, P. Yu, L. O. Alimi, B. A. Moosa, J. L. Sessler and N. M. Khashab, *J. Am. Chem. Soc.*, 2023, **145**, 12609–12616.
44 N. J. Heo, V. M. Lynch, D. E. Gross, J. L. Sessler and S. K. Kim, *Chem.–Eur. J.*, 2023, e202302410.